NJC

Accepted Manuscript

This is an *Accepted Manuscript*, which has been through the Royal Society of Chemistry peer review process and has been accepted for publication.

Accepted Manuscripts are published online shortly after acceptance, before technical editing, formatting and proof reading. Using this free service, authors can make their results available to the community, in citable form, before we publish the edited article. We will replace this *Accepted Manuscript* with the edited and formatted *Advance Article* as soon as it is available.

You can find more information about *Accepted Manuscripts* in the Information for Authors.

Please note that technical editing may introduce minor changes to the text and/or graphics, which may alter content. The journal's standard Terms & Conditions and the Ethical guidelines still apply. In no event shall the Royal Society of Chemistry be held responsible for any errors or omissions in this *Accepted Manuscript* or any consequences arising from the use of any information it contains.

ROYAL SOCIETY OF CHEMISTRY

www.rsc.org/njc

Surfactant-assisted hydrothermal synthesis of ultrafine $CoMoO_4 \cdot 0.9H_2O$ nanorods towards high-performance supercapacitors

Linrui Hou [a,] **, Hui Hua* [a], *Sijia Liu* [a], *Gang Pang,* [a] *Changzhou Yuan* [a, b] ***

[a] *School of Materials Science & Engineering, Anhui University of Technology, Ma'anshan, 243002, P.R. China*

[b] *Chinese Academy of Science (CAS) Key Laboratory of Materials for Energy Conversion, Hefei, 230026, P.R. China*

Email: hour629@163.com (L.R. Hou); ayuancz@163.com (C.Z. Yuan)

Abstract

In the study, one-dimensional (1D) $CoMoO_4 \cdot 0.9H_2O$ nanorods (NRs) with different sizes and crystallinities were controllably fabricated *via* facile hydrothermal strategy coupled with the assistance of various surfactants, and further utilized as electroactive materials for supercapacitors. The significant influences of surfactants upon the crystalline phases, sizes and electrochemical performance of the resulting $CoMoO_4 \cdot 0.9H_2O$ were systematically investigated. Physicochemical characterizations demonstrated that the 1D NRs product (denoted as CMO-CTMAB) synthesized by using hexadecyl trimethyl ammonium bromide (CTMAB) was endowed with the weakest crystallization, minimum size (~10 nm) and highest specific surface area (~98 $m^2\ g^{-1}$), when compared to other anionic and/or non-ionic surfactants. Benefiting from its weak crystallization, large electroactive surface, and 1D nanoscaled architecture, the ultrafine CMO-CTMAB NRs manifested excellent electrochemical capacitance with the largest specific capacitance (SC) of 377 F g^{-1} and high SC retention (~93%) in 2 M KOH up to 1000 cycles at the current rate of 0.5 A g^{-1}.

Keywords: $CoMoO_4 \cdot 0.9H_2O$ nanorods; One-dimensional nanostructures; Surfactants; Supercapacitors; Pseudo-capacitance

1. Introduction

To address the rapid increasing global energy consumption along with the critical issue of climate change, it is urgent and of great significance to develop more environment friendly and sustainable energy-storage systems.[1, 2] As intermediate devices to second batteries and physical capacitors, supercapacitors exhibit several desirable properties, including high power density, fast charging/discharging, long cycling life, high safety, *etc.*, which render it one of the most promising candidates for next-generation power devices.[1-4] Unfortunately, the low specific capacitance (SC) is still far from perfect considering the ever-growing need for peak-power assistance in electric vehicles (EVs) and/or hybrid EVs. As a consequence, growing interest in utilizing pseudo-capacitive materials has been triggered for high-performance supercapacitors. Recently, transitional metal oxides (TMOs), possessing multiple oxidation states towards rich redox reactions for pseudo-capacitance, have drawn extensive attention in supercapacitors as appealing electrode materials.[1] In particular, mixed transitional metal oxides (MTMOs) have been retrieved so far to exhibit even better electrochemical performance than any single component, thanks to their versatile oxidation states and higher electronic conductivity, and so on.[1-6]

Among available MTMOs, metal molybdates, especially cobalt molybdate ($CoMoO_4$) has exhibited prominent advantages for high-performance supercapacitors, benefiting from their attracting electrical conductivity and superior pseudo-capacitive activity.[3-6] As is well known, the electrochemical performance of pseudo-capacitive materials was generally determined by their electrochemically kinetic feature, according to their unique charge-storage mechanisms. For remarkable enhancement in electrochemical kinetics inside the electrode and/or the electrode/electrolyte sur-/interface, an efficient strategy is to fabricate one-dimensional (1D) electroactive

nano-architectures,[3, 5-9] since such unique 1D structure can provide short diffusion path lengths for the electron and electrolyte ions, resulting in large SCs at high charge/discharge rates.

As retrieved, Mai *et al.*[3] synthesized well-crystalline $CoMoO_4$ NRs with a size of ~50 nm, however, a low SC of ~62.8 F g^{-1} was just obtained at a current density of 1 A g^{-1}. Following this pioneer work, Kong and co-authors[6] developed chemical co-precipitation route to prepare hybrid $CoMoO_4/CoMoO_6{\cdot}0.9H_2O$ NRs with size range from 100 to 300 nm, and a SC of 286 F g^{-1} was obtained at ~0.5 A g^{-1}. The same group further fabricated $CoMoO_4{\cdot}0.9H_2O$ NRs of 100 – 150 nm in size *via* hydrothermal method, and a SC of ~326 F g^{-1} (~0.5 A g^{-1}) was delivered accordingly.[5] Although these electrochemical properties mentioned above are still unsatisfactory, particularly at high rates, these findings explicitly suggest that hydrated $CoMoO_4$ NRs demonstrate even better electrochemical behaviors, and the electrochemical capacitance of the $CoMoO_4$-based electrodes depends significantly upon their crystallization and size. As well established, finer structures with larger surface to volume ratios are desirable for enhancing electrochemical activities of electroacitve materials.[1, 4, 5, 7] Therefore, it is of great importance to explore simple protocols to effectively adjust the specific crystallization and dimensions of the nanophase hydrate $CoMoO_4$ with the ultimate aim to optimize its electrochemical capacitance, particularly at high current densities.

With aforementioned considerations in mind, herein, a simple hydrothermal strategy with the assistance of various surfactants was purposefully developed to fabricate 1D $CoMoO_4{\cdot}0.9H_2O$ NRs with adjustable sizes and crystallinities. Physicochemical and electrochemical characterizations revealed that the 1D $CoMoO_4{\cdot}0.9H_2O$ NRs synthesized by using the cationic hexadecyl trimethyl

ammonium bromide (CTMAB) demonstrated the weakest crystallization, minimum size and the highest specific surface area (SSA), and delivered excellent electrochemical capacitance with the largest SC of 377 F g^{-1} and high SC retention (~93%) in 2 M KOH aqueous electrolyte over 1000 cycles at the current density of 0.5 A g^{-1}, when estimated as an electroactive material for supercapacitors.

2. Experimental

Materials Synthesis. All the chemicals used here were of analytical grade, and used as received without further purification. In a typical procedure, 0.3 g of $CoCl_2 \cdot 6H_2O$ and 0.305 g of $Na_2MoO_4 \cdot 2H_2O$ were separately dissolved in 15 mL of CTMAB aqueous solution (0.01 M) under magnetic stirring. Then, the above two solutions were mixed together to form a homogeneous solution, and subsequently transferred into a Teflon-lined stainless autoclave. The autoclave was sealed, maintained at 120 ºC for 6 h, and then cooled to room temperature (RT). Afterwards, the precipitate was filtered, washed with excess distilled water and absolute ethanol, and dried in vacuum at 60 ºC for 8 h. For comparison, other surfactants including sodium dodecyl sulfate (SDS), polyethylene glycol 4000 (PEG), polyethylene glycol octylphenol ether (PGOE), and polyvinylpyrrolidone (PVP, M.W. 45000 ~ 50000) were applied to prepare other samples instead of the CTMAB. For convenience, the as-prepared products by using CTMAB, SDS, PEG, PGOE, PVP, and without any surfactant were designed as CMO-CTMAB, CMO-SDS, CMO-PEG, CMO-PGOE, CMO-PVP and CMO, respectively.

Materials Characterization. Crystallographic phase of the products was investigated by powder X-ray diffraction (XRD) (Max 18 XCE, Japan) by using a Cu K*a* source (λ = 0.154056 nm) at a scanning speed of 3° min^{-1} over a 2θ range of 10 – 80 °. The morphologies and microstructures were observed by using field-emission scanning

electron microscopy (FESEM, JEOL-6300F, 15 kV), transmission electron microscope (TEM), and high-resolution transmission electron microscopy (HRTEM) (JEOL JEM 2100 system operating at 200 kV). Measurement of SSA for all the resulting products was performed through measuring N_2 adsorption-desorption isotherms at 77 K with an ASAP-2010 surface area analyzer.

Electrochemical Measurements. Electrochemical measurements were carried out in a three-electrode electrochemical cell containing 2 M KOH aqueous solution as the electrolyte at RT. The working electrode was prepared by mixing 85 wt.% of the resultant products, 5 wt.% of acetylene black and 10 wt.% of poly(tetrafluoroethylene). And the mixture was pressed onto a nickel grid (7 MPa). Electrochemical performance was evaluated in 2 M KOH on IVIUM electrochemical workstation by cyclic voltammetry (CV), chronopotentiometric (CP) charge-discharge and electrochemical impedance spectroscopy (EIS) measurements with a Pt foil and a saturated calomel electrode (SCE) as counter electrode and reference electrode, respectively. The typical loading of each electrode is 8.5 mg cm^{-2}. The SCs of electrodes were calculated from the following equation:

$$SC = \frac{I \times \Delta t}{\Delta V} \qquad (1)$$

where I, Δt and ΔV are the discharge current (A g^{-1}), the discharge time (s) and the charge/discharge potential window (V), respectively. And the EIS "small-signal" capacitance of the electrode can be calculated from the imaginary component of the impedance by using the equation:[10]

$$SC = \frac{1}{-2\pi f Z``m} \qquad (2)$$

where f is the frequency (0.01 Hz), m the mass of electroactive material in each electrode, and $Z``$ the imaginary component of impedance at frequency (f = 0.01 Hz).

3. Results and Discussion

3.1 Physicochemical characterizations

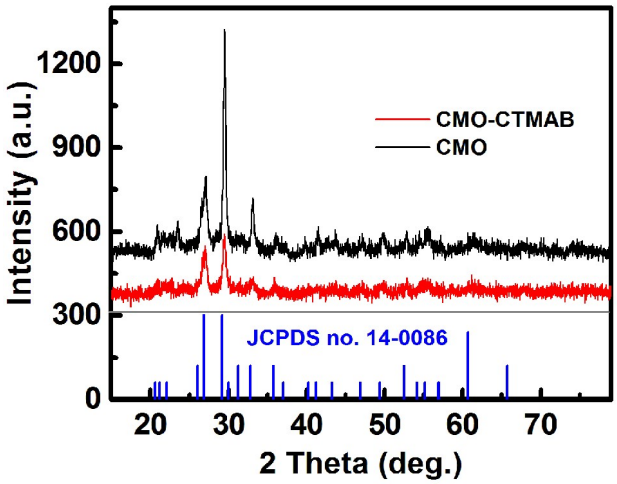

Fig. 1. XRD patterns of the as-prepared CMO-CTMAB and CMO products

Herein, we fabricate the CMO-CTMAB by using $CoCl_2 \cdot 6H_2O$ and $Na_2MoO_4 \cdot 2H_2O$ as the raw materials and CTMAB as surfactant *via* hydrothermal treatment at 120 ºC for 6 h. As is known to all, it is difficult to achieve phase-pure $CoMoO_4$ *via* a wet chemistry approach owing to the formation of hydrates by the intercalation of water molecules between the inter-layers.[11, 12] As expected, hydrated $CoMoO_4$ was obtained accordingly. Typical crystal phase and structure information of the samples was derived by XRD measurement. **Fig. 1** shows the typical XRD patterns of as-obtained CMO and CMO-CTMAB samples. Apparently, all the observed Bragg reflection peaks for the two products can be unambiguously assigned to the $CoMoO_4 \cdot 0.9H_2O$ phase (JCPDS card no: 14-0086), as indicated by the blue vertical lines in **Fig. 1**, and no peaks originating from other impurities can be identified. Compared to the CMO, the resultant CMO-CTMAB strikingly exhibit broad and weak diffraction peaks, suggesting smaller crystallite size and weaker crystallization of the resultant CMO-CTMAB sample, which are strongly favorable for enhancing its electrochemical capacitive behaviors.[5, 6]

For comparison, a series of parallel experiments were carried out by using other surfactants under otherwise identical condition used. **Fig. 2** displays the representative XRD patterns of the resulting samples by using other surfactants, such as SDS, PEG, PGOE and PVP. Obviously, the main peak positions of the five samples show no any discernible changes, illustrating the same $CoMoO_4 \cdot 0.9H_2O$ phase for all the products. After careful examination, it is easy to find that the diffraction intensities (2θ = 29.4 º) of these products are different from each other, and corresponding data are collected in **Table S1** (Electronic Supporting Information, ESI†). Note that the variation tendency of the diffraction intensity follows the sequence as below: CMO-CTMAB (~240) < CMO-SDS (~433) < CMO-PEG (~542) < CMO-PGOE (~642) < CMO (~747) < CMO-PVP (~813). Obviously, with the surfactants, the crystallinity of the resultant samples turns out to be even weaker just with the exception of PVP, and the products prepared by using non-ionic surfactants illustrates much better crystallinity than those synthesized by ionic surfactants (such as, CTMAB and SDS). Of particular note, the CMO-CTMAB demonstrates the lowest diffraction intensity among these products when the cationic CTMAB was applied, even less than that for the anionic SDS, suggesting the weakest crystalline nature of the CMO-CTMAB.

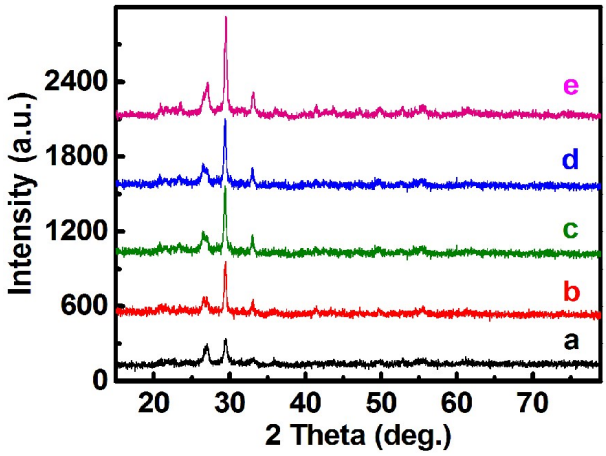

Fig. 2. XRD patterns of the CMO-CTMAB (a), CMO-SDS (b), CMO-PEG (c), CMO-PGOE (d) and CMO-PVP (e), respectively

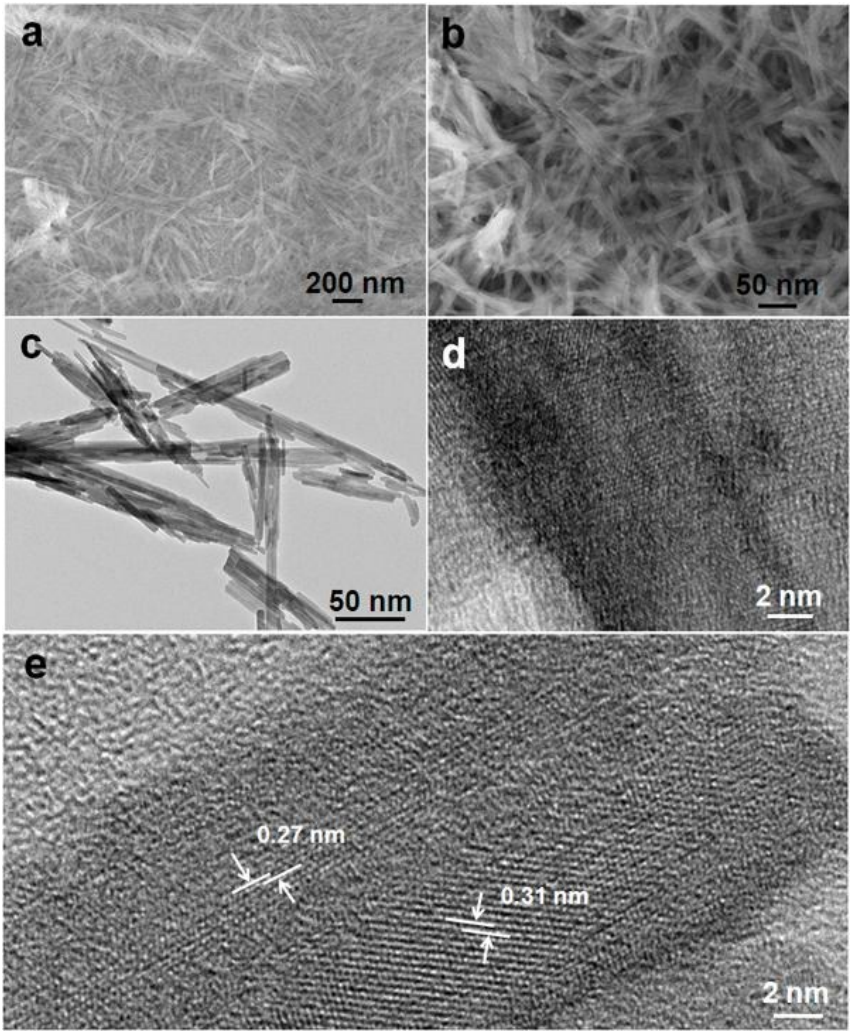

Fig. 3. FESEM (a, b), TEM (c) and HRTEM (d, e) images of the CMO-CTMAB NRs

Fig. 3a demonstrates the typical FESEM images of the as-obtained CMO-CTMAB. As seen in **Fig. 3a**, the CMO-CTMAB product is composed entirely of NRs with a length of ~400 nm. A close examination (**Fig. 3b**) reveals that the NRs are generally aggregated to form loose bundles, owing to their high surface energy. As illustrated in **Fig. 3c**, some aggregated rod-like bundles are evidently presented for the CMO-CTMAB sample, in good accordance with the FESEM observation above, and the diameter of NRs is estimated as ~10 nm. **Fig. 3d** shows the typical HRTEM image of a single NR. Blurry lattice finger apparently reveals the modest crystalline nature of the CMO-CTMAB itself, resulting from the rich defects and dislocations retained in the resulting NRs. Additionally, two overlapped NRs with ill-defined boundary are

clearly observed in **Fig. 3e**. Although weak crystallization is presented yet, two adjacent lattice fringes of ~0.27 and ~0.31 nm still can be seen, unfortunately, which cannot be indexed successfully to any planes of the $CoMoO_4 \cdot 0.9H_2O$, owing to its uncertain crystal structure in nature.[5] In contrast, as for the case with the absence of CTMAB, the length of the resultant CMO specimen (**Fig. S1a**, **b**; ESI†) is ranged from several hundreds of nanometers to ~25 μm, and their mean diameter increases up to ~200 – 500 nm, although NR-like feature remains discernible.

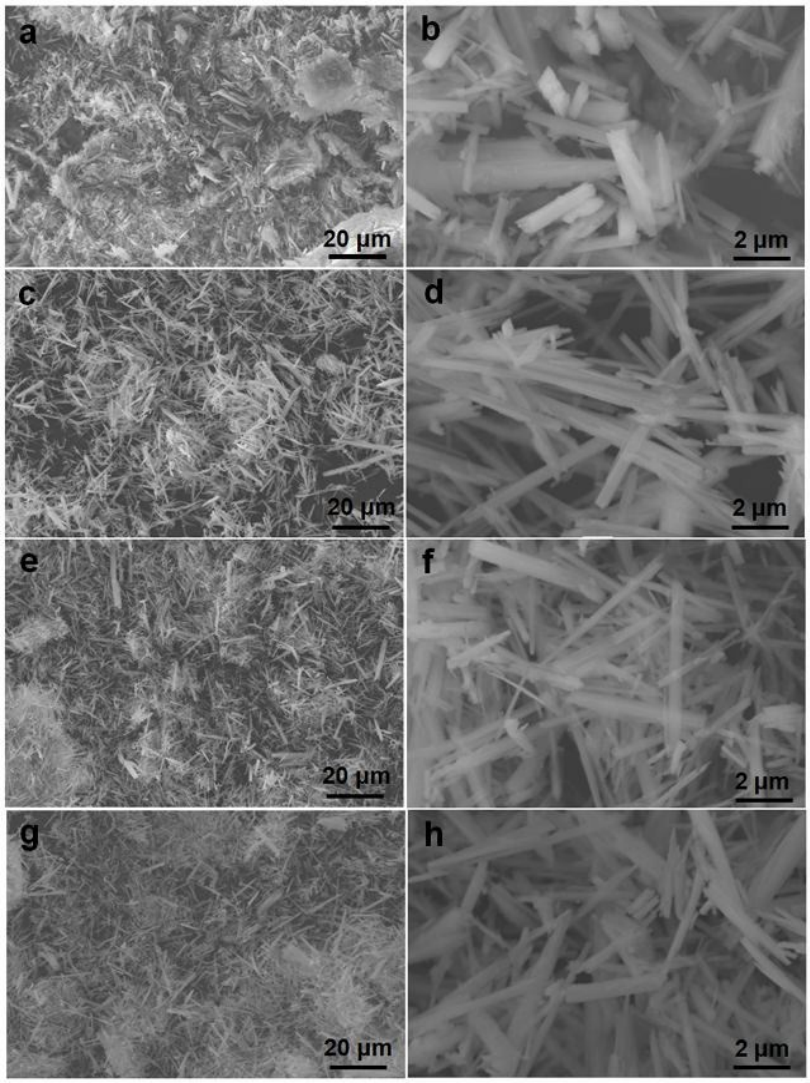

Fig. 4. FESEM images of CMO-SDS (a, b), CMO-PEG (c, d), CMO-PGOE (e, f) and CMO-PVP (g, h)

Fig. 4 demonstrates the FESEM images of the products synthesized by using

other surfactants. As observed in **Fig. 4a**, the CMO-SDS just consists of a great number of irregular NRs in an aggregated state. The magnified image (**Fig. 4b**) further indicates that CMO-SDS sample is extremely un-uniform, and presented with the length of 1 ~ 4 μm and the diameter of 0.2 ~ 2 μm. While as regards other samples prepared in the presence of PEG, PGOE and PVP, all of them show rod-like structures (**Fig. 4c-h**). As can be seen from **Fig. 4c**, **d**, the CMO-PEG is obviously composed of lots of NRs with an average length of ~30 μm and a mean diameter of ~500 nm. As to the CMO-PGOE, some NRs are evident with lengths of up to several tens of micrometers, and diameter range from 100 to 500 nm, as seen in **Fig. 4e**, **f**. When the surfactant of PVP was further used, the CMO-PVP demonstrates no obvious change in morphology (**Fig. 4g**, **h**), compared to that for the CMO-PGOE. And the SSA can be calculated as ~73, ~98, ~92, ~87, ~72 and ~70 $m^2 g^{-1}$ for the as-synthesized CMO, CMO-CTMAB, CMO-SDS, CMO-PEG, CMO-PGOE and CMO-PVP, respectively.

Based on the above observations, it is easy to conclude that the crystallinity and dimensions of the resultant samples can be efficiently regulated just by selecting different surfactants, and the ionic surfactants show stronger influence upon the dimensions of the as-synthesized samples. In particular, the cationic surfactant of CTMAB plays a significant role in fabricating ultrafine CMO-CTMAB NRs with modest crystalline, the smallest diameter and the highest SSA. Noticeably, such unique structure feature would ensure the facility of electrolyte penetration and high electroactivity of the CMO-CTMAB electrode, rendering it a promising electrode candidate for high-performance supercapacitors.

3.2 Electrochemical properties

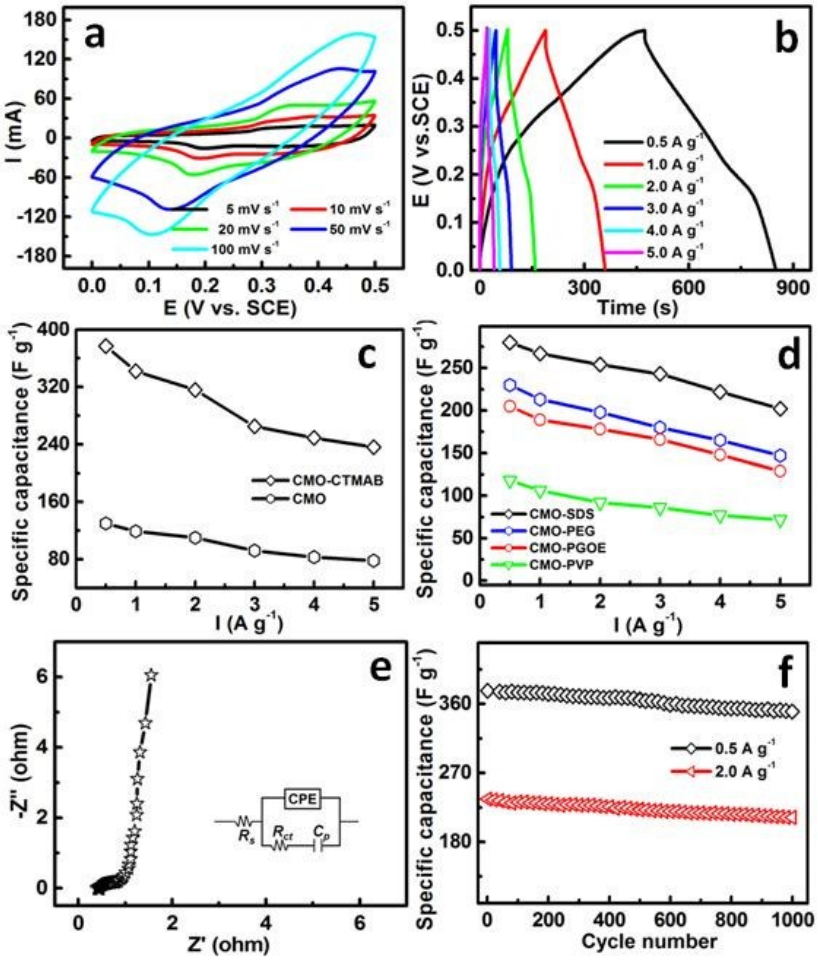

Fig. 5. CV curves (a), charge/discharge plots (b), SC as a function of current density (c), EIS data (e) and cycling performance (f) for the CMO-CTMAB NRs, and SC as a function of current rate for other CMO sample as indicated. The inset in panel (e) for the fitting circuit for the EIS of the CMO-CTMAB

To further check the optimized electrochemical performance of the as-prepared electrodes for advanced supercapacitors, the CMO-CTMAB sample was first applied as a model electrode, and **Fig. 5a** depicts its typical CV curves at various sweep rates in a three-electrode cell by using 2 M KOH as the electrolyte. It is noteworthy that a pair of well-defined redox peaks are observed explicitly in all the CV curves at wide scan rate range from 5 to 100 mV s^{-1}, suggesting that the capacitive characteristics of the CMO-CTMAB are intrinsically governed by the typical Faradaic redox reactions originating from the charge-transfer kinetics of Co^{2+}/Co^{3+} in the electrode, that is, the

electrochemical capacitance of the CMO-CTMAB electrode should be mainly attributed to the quasi-reversible electron transfer process that mainly involves the Co^{2+}/Co^{3+} redox couple, and probably mediated by the OH^- ions in 2 M KOH, which is consisted with the previous reports.[3-6, 13, 14] Furthermore, as the scan rate increases, the current is subsequently up while the CV shape changes little, even at a scan rate as high as 100 mV s^{-1}, which strongly suggests that the fast kinetics of the sur-/interfacial Faradaic reactions and the rapid rates of electronic and ionic transport for the CMO-CTMAB electrode at large-current charge/discharge process.

To further qualify the SCs of the unique CMO-CTMAB sample, CP measurement at various mass-normalized current densities ranged from 0.5 to 5 A g^{-1} is carried out with a maximum electrochemical window of 0.5 V (*vs.* SCE), and typical charge-discharge curves are plotted in **Fig. 5b**. Evidently, the nonlinear charging/discharging plots are shown clearly, and reveal typical Faradaic redox reactions occurring at electrode/electrolyte sur-/interfaces, verifying its typical pseudo-capacitive characteristic in aqueous KOH once again, which is in good agreement with the above CV data (**Fig. 5a**). Based on the CP data, the SCs of the ultrafine CMO-CTMAB electrode are calculated and summarized in **Fig. 5c**. The unique 1D CMO-CTMAB electrode delivers SCs as large as ~377, ~342, ~316, ~265, ~249 and ~236 F g^{-1} at current densities of 0.5, 1, 2, 3, 4 and 5 A g^{-1}, respectively, which suggests that ~63 % of the initial SC is still maintained when the charge-discharge rate is increased from 0.5 to 5 A g^{-1}. The 1D ultrathin NR feature observed here for the CMO-CTMAB allows rapid transportation of electrolyte ions into its bulk with weak crystallinity, which is in favor of improving its rate capability.

In addition, calculation of the pure electric double layer capacitance (EDLC) by using an average value of 20 μF cm^2 [10, 15] gives an EDLC of ~20 F g^{-1} for such

ultrafine CMO-CTMAB NRs, much lower than the measured SC of 377 F g^{-1} at the current rate of 0.5 A g^{-1} (~4.25 mA cm^{-2}). Thus, the main contribution to the calculated SC should be from the pseudo-capacitive surface redox process, and the Faradaic SC is estimated as ~357 F g^{-1} (corresponding to a area SC of ~3.6 F m^{-2}) accordingly, verifying its high electrochemical utilization. As a contrast, the pseudo-capacitive SC of the CMO is calculated as ~116 F g^{-1} (just ~1.6 F m^{-2}) at 0.5 A g^{-1}, and when the current is up to 5 A g^{-1}, a SC as low as ~64 F g^{-1} is just delivered. It is also worthy of noting that the SC value calculated for CMO-CTMAB is greatly larger than those for the CMO-SDS (280 F g^{-1}), CMO-PEG (230 F g^{-1}), CMO-PGOE (205 F g^{-1}) and CMO-PVP (128 F g^{-1}) at the same current density of 0.5 A g^{-1}, as seen in **Fig. 5d**. Accordingly, the pseudo-capacitive area SCs of CMO-SDS, CMO-PEG, CMO-PGOE and CMO-PVP electrodes are calculated as ~2.8, ~2.4, ~2.7 and ~1.6 F m^{-2}, respectively. This observation strongly confirms the superior surface utilization of the CMO-CTMAB electrode for electrochemical energy storage in KOH aqueous electrolyte again. More attractively, the SCs estimated here for the 1D CMO-CTMAB NRs are even higher than those for other $CoMoO_4$ samples,[3, 5, 14, 16, 17] $CoMoO_4 \cdot 0.9H_2O$ NRs,[4] $CoMoO_4 \cdot 0.75H_2O$ NRs,[18] and Co_3O_4[19, 20] and $Co(OH)_2$[21-23]. Interestingly, the SC of the CMO-PGOE (~136 F g^{-1} at 5 A g^{-1}) is greatly higher than those of the CMO (~78 F g^{-1}) and CMO-PVP (~71 F g^{-1}) products at the same rate, while all the three present very close SSA of ~70 m^2 g^{-1}. With the obvious differences among the three samples in mind, one should note that the modest crystallinity of the CMO-PGOE itself should be responsible well for its larger electrochemical capacitance than the other two. The similar phenomenon also can be observed for the case of the CMO-CTMAB and CMO-SDS.

To further investigate the electrochemical process of the CMO-CTMAB

electrode for rapid Faradaic energy storage, EIS analysis of 1D CMO-CTMAB electrode was conducted at the 0.45 V (*vs.* SCE) in the frequency range of 0.01 – 10^5 Hz with an AC signal amplitude of 5 mV. The obtained EIS in terms of Nyquist plot typically (-Z`` *vs.* Z`) and the corresponding fitting circuit (the inset) were given in **Fig. 5e**. The intersection of the plots at the X-axis represents solution resistance (R_s),[11, 24, 25] which is associated with three contributions from the contact resistance at the interface between electroactive material and current collector, the resistance of the KOH solution and the intrinsic resistance of the electroactive material. Clearly, R_s is just as small as ~0.4 Ohm, revealing good electronic conductivity of the 1D NRs. At the high-medium frequency region, a typical semicircle standing for the charge transfer resistance (R_{ct}) in the electrochemical process can be found. And the R_{ct} is around 0.6 Ohm. Such low values mean the small R_s and R_{ct} of the CMO-CTMAB electrode during the redox process for efficient energy storage. Additionally, the nearly vertical line leaning to imaginary axis observed in the low-frequency region indicates the rapid electrolyte ions diffusion to the electroactive material and ideal supercapacitive behavior due to its unique 1D architecture. As a consequence, the EIS "small-signal" capacitance of the 1D CMO-CTMAB NRs can be calculated as ~331 F g^{-1} (f = 0.01 Hz) from the imaginary component of the EIS data.

The long-term cycling stability is another critical requirement for practical supercapacitors application. **Fig. 5f** depicts the SC variation as a function of the cycle number at different current densities of 0.5 and 2 A g^{-1}, respectively, for up to 1000 cycles. It can be detected easily that the SCs of the CMO-CTMAB electrode gradually reduce, whereas the SC degradations of ~7% and ~11% still can be observed at 0.5 and 2 A g^{-1} over continuous 1000 cycles, suggesting its stable cycling property even at large current density. The electrochemical data mentioned above further highlights the

remarkable merits of the CMO-CTMAB as an high-performance electrode to meet the requirements of both long cycling lifetime and large SCs at high rates, which should be attributed to the modest internal resistance and small charge-transfer resistance of the 1D ultrafine NRs with weak crystallization and rich electroactive sites.

4. Conclusions

In conclusion, we successfully developed an efficient surfactant-assisted hydrothermal methodology to controllably fabricate 1D $CoMoO_4 \cdot 0.9H_2O$ NRs with different sizes and crystallinities. The significant influence of surfactants upon the crystal phases and sizes of the resulting $CoMoO_4 \cdot 0.9H_2O$ was investigated in detail. The CMO-CTMAB of ~10 nm in size was synthesized by using cationic surfactant of CTMAB, and demonstrated the weakest crystallization, minimum size and highest SSA, compared to other anionic and/or non-ionic surfactants. When utilized as electrodes for supercapacitors, the ultrafine CMO-CTMAB NRs delivered appealing electrochemical capacitance in 2 M KOH even at high rates, thanks to its weak crystallization, large electroactive surface and 1D nanoscaled architecture. Taking advantage of its excellent electrochemical capacitance, low cost, and easy fabrication, the findings here demonstrate the CMO-CTMAB NRs would be a promising and scalable alternative electrode material for next-generation supercapacitors.

Acknowledgements

The authors acknowledge the financial support from National Natural Science Foundation of China (no. 51202004), Anhui Province Funds for Distinguished Young Scientists (no. 1508085J09), the Natural Science Foundation of Anhui Province (no. 1508085ME106, KJ2013A051), the Foundation for Young Talents in College of Anhui Province, and the Opening Project of CAS Key Laboratory of Materials for

Energy Conversion (no. 2014001).

Supporting Information

FESEM images, XRD diffraction intensity and BET SSA data of the samples are available.

References

[1] C. Z. Yuan, H. B. Wu, Y. Xie and X. W. Lou, *Angew. Chem. Int. Ed.*, 2014; **53**, 1488.

[2] C. Liu, F. Li, L. P. Ma and H. M. Cheng, *Adv. Mater.*, 2010, **22,** E28.

[3] L. Q. Mai, F. Yang, Y. L. Zhao, X. Xu, L. Xu and Y. Z. Luo, *Nature Commun.*, 2011, **2**, 381.

[4] X. Z. Yu, B. G. Lu and Z. Xu, *Adv. Mater.*, 2014, **26**, 1044.

[5] M. C. Liu, L. B. Kong, X. J. Ma, C. Lu, X. M. Li, Y. C. Luo and L. Kang, *New J. Chem.*, 2012, **36**, 1713.

[6] M. C. Liu, L. B. Kong, C. Lu, Y. Q. Dou, X. M. Li and Y. C. Luo and L. Kang, Mater. Lett., 2013, 94, 197.

[7] C. Z. Yuan, J. Y. Li, L. R. Hou, L. Yang, L. F. Shen and X. G. Zhang, *J. Mater. Chem.*, 2012, **22**, 16084.

[8] R. Liu and S. B. Lee, *J. Am. Chem. Soc.*, 2008, **130**, 2942.

[9] L. Yu, G. Q. Zhang, C. Z. Yuan and X. W. Lou, *Chem. Commun.*, 2013, **49**, 137.

[10] C. Z. Yuan, J. Y. Li, L. R. Hou, J. D. Lin, X. G. Zhang and S. L. Xiong, *J. Mater. Chem. A*, 2013, **1**, 11145.

[11] G. K. Veerasubramani, K. Krishnamoorthy, S. Radhakrishnan, N. J. Kim and S. J. Kim, *Int. J. Hydrogen energy*, 2014, **39**, 5186.

[12] J. L. Brito and A. L. Barbosa, *J. Catal.*, 1997, **171**, 467.

[13] D. Guo, H. M. Zhang, X. Z. Yu, M. Zhang, P. Zhang, Q. H. Li and T. H. Wang, *J. Mater. Chem. A*, 2013, **1**, 7247.

[14] X. F. Xia, W. Lei, Q. L. Hao, W. J. Wang and X. Wang, *Electrochim. Acta*, 2013, **99**, 253.

[15] H. Q. Li, J. Y. Luo and Y. Y. Xia, *J. Electrochem. Soc.*, 2007, **154**, A731.

[16] X. W. Xu, J. F. Shen, N. Li and M. X. Ye, *J. Alloy. Compd.*, 2014, **616**, 58.

[17] Z. W. Xu, Z. Li, X. H. Tan, C. M. B. Holt, L. Zhang, B. S. Amirkhiz and D. Mitlin, *RSC Adv.*, 2012, **2**, 2753.

[18] M. Mandal, D. Ghosh, S. Giri, I. Shakir and C. K. Das, *RSC Adv.*, 2014, **4**, 30382.

[19] M. B. Zheng, J. Cao, S. T. Liao, J. S. Liu, H. Q. Chen, Y. Zhao, W. J. Dai, G. B. Ji, J. M. Cao and J. Tao, *J. Phys. Chem. C*, 2009, 113, 3887.

[20] S. L. Xiong, C. Z. Yuan, X. G. Zhang, B. J. Xi and Y. T. Qian, *Chem. Eur. J.*, 2009, **15**, 5320.

[21] W. J. Ren, D. Guo, M. Zhuo, B. K. Guan, D. Zhang and Q. H. Li, *RSC Adv.*, 2015, **5**, 21881.

[22] C. Z. Yuan, X. G. Zhang, B. Gao and J. Li, *Mater. Chem. Phys.*, 2007, **101**, 148.

[23] C. H. Chen, D. S. Tsai, W. H. Chung, K. Y. Lee, Y. M. Chen and Y. S. Huang, *J. Power Sources*, 2012, **205**, 510.

[24] A. Chu and P. Braatz, *J. Power Sources*, 2002, **112**, 236.

[25] C. Z. Yuan, X. G. Zhang, L. R. Hou, L. F. Shen, D. K. Li, F. Zhang, C. G. Fan and J. M. Li, *J. Mater. Chem.*, 2010, **20**, 10809.